Comparison of the Backbone Dynamics of a Folded and an Unfolded SH3 Domain Existing in Equilibrium in Aqueous Buffer†

Neil A. Farrow,*,‡ Ouwen Zhang,‡,§ Julie D. Forman-Kay,§,|| and Lewis E. Kay*,‡

Protein Engineering Network Centres of Excellence and Departments of Medical Genetics, Biochemistry, and Chemistry, University of Toronto, Toronto, Ontario M5S 1A8, Canada, and Biochemistry Research Division, Hospital for Sick Children, 555 University Avenue, Toronto, Ontario M5G 1X8, Canada

Received October 3, 1994⊗

ABSTRACT: Two-dimensional NMR ^{15}N relaxation studies have been used to characterize the backbone dynamics and folding transition of the N-terminal SH3 domain of the protein drk (drkN SH3). The isolated drkN SH3 domain exists in equilibrium between a folded and an unfolded state in aqueous buffer and near neutral pH [Zhang et al. (1994) *J. Biomol. NMR 4*, 845]. The backbone dynamics of both the folded and unfolded states in this exchanging system have been determined and the rates of the folding transition estimated at 14 °C. For 12 residues, the values of the spectral density functions of the backbone amide bond vectors at a number of frequencies have been established. Results show that while the unfolded state has considerably greater dynamic behavior, the overall motional properties are consistent with it having a reasonably compact structure in solution. In contrast to the folded state, considerable variations are seen in the values of the spectral densities of the unfolded state as a function of residue number; these variations do not appear to be strongly correlated with structural elements in the folded state. The mean value of the exchange rate associated with the folding transition was determined to be 0.89 s^{-1}, similar to previous measurements of the rate of formation of β-structure.

In recent years there has been an increased emphasis on understanding the physical nature of the unfolded state of proteins since it has been recognized that this will assist in the elucidation of the mechanisms by which proteins fold to their native state [for review see Shortle (1993)]. Many proteins can be reversibly unfolded upon the addition of denaturants such as urea or guanidine hydrochloride or through extremes of either temperature or pH. Characterization of the unfolded states of these proteins has revealed that denatured proteins often contain residual structure and exist in compact configurations. However, interpretation of the relationship between denaturant-induced unfolded states and naturally occurring unfolded states is complicated by the observed sensitivity of the denatured state to the conditions of denaturation and by the nonphysiological effects of the denaturants.

Recently, the equilibrium between a folded and an unfolded form of the N-terminal SH3[1] domain of the *Drosophila* signal transduction protein drk (drkN SH3) in aqueous buffer and near neutral pH has been described (Zhang & Forman-Kay, 1995). Structural characterization of the folded form based on NOE connectivities, secondary chemical shifts, $^3J_{HN\alpha}$ coupling constants, and amide exchange rates demonstrates that the folded form of the drkN SH3 domain adopts a tertiary structure similar to that described for other SH3 domains [for review see Kuriyan and Cowburn (1993)]. A model of the proposed structure of the drkN SH3 domain based on the structure of the N-terminal SH3 domain of grb2 (Wittekind et al., 1994), the mammalian homologue of the drk protein, is shown in Figure 1. This model is consistent with current structural data on the folded state of the drkN SH3 domain. Studies of the unfolded form of the drkN SH3 domain using ^{15}N-edited NMR experiments reveal an absence of long range NOEs indicating loss of tertiary structure. Interestingly, stretches of weak NH_i-NH_{i+1} NOE connectivities between residues 35−47 and residues 52−54 were observed in the unfolded state. While these NOEs may be indicative of a preferential sampling of the α-helical region of conformational space, the fact that they are weak and the observation of considerably stronger $C\alpha H_i-NH_{i+1}$ NOEs and values of $^3J_{HN\alpha}$ couplings of 6−7 Hz in the same region of the molecule suggest that any structure that this region adopts is transient and in rapid exchange with other conformations. A number of observations indicate that the conformational exchange between the two states observed in this system is identical to the folding/unfolding transition of the drkN SH3 domain in aqueous solution. Principal among these is the fact that the unfolded form of the domain is in exchange with the folded form at a rate of approximately 1 per second (see below), similar to rates measured for the folding of other predominantly β-sheet proteins (Varley et al., 1993). Fur-

† This work was supported through grants from the Natural Sciences and Engineering Research Council of Canada (L.E.K.) and the National Cancer Institute of Canada (J.D.F.-K. and L.E.K.) with funds from the Canadian Cancer Society. N.A.F. is a Research Fellow of the National Cancer Institute of Canada supported with funds provided by the Canadian Cancer Society. O.Z. acknowledges a graduate fellowship from the University of Toronto.

‡ Protein Engineering Network Centres of Excellence and Departments of Medical Genetics, Biochemistry, and Chemistry, University of Toronto.

§ Hospital for Sick Children.

|| Department of Biochemistry, University of Toronto.

⊗ Abstract published in *Advance ACS Abstracts,* December 15, 1994.

[1] Abbreviations: SH3, Src homology 3; NMR, nuclear magnetic resonance; CPMG, Carr−Purcell−Meiboom−Gill; BPTI, bovine pancreatic trypsin inhibitor; NOE, nuclear Overhauser effect; FKBP, FK506 binding protein; HSQC, heteronuclear single quantum coherence; ω_N, Larmor frequency of ^{15}N; ω_H, Larmor frequency of ^1H.

0006-2960/95/0434-868$09.00/0

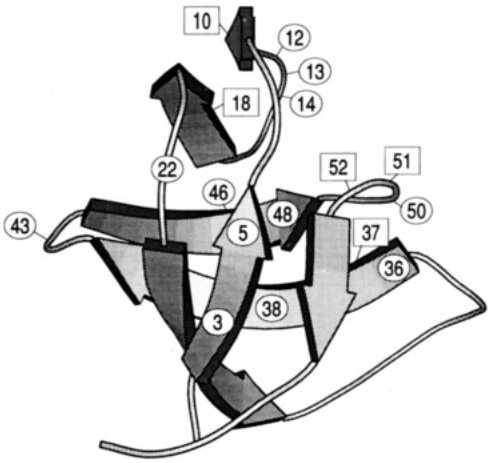

FIGURE 1: Schematic diagram of a model of the structure of the drkN SH3 domain based upon homology to the NMR-derived structure of the N-terminal SH3 domain of grb2 (Wittekind et al., 1994). The positions of residues discussed in this study are indicated. Residues for which equilibrium constants and spectral density functions were calculated are indicated by ellipses. Residues for which only equilibrium constants were obtained are indicated by rectangles. References to individual β-strands in the text are made by numbering the strands sequentially from the N-terminus. The figure was generated using the program Molscript (Kraulis, 1991).

thermore, the chemical shifts of the folded form are identical to those of the fully folded state obtained in the presence of 0.4 M Na_2SO_4, while the chemical shifts of the unfolded form are similar to those observed in the presence of 2 M guanidine hydrochloride. Note that the SO_4^{2-} anion is at one extreme of the Hofmeister series of anions and therefore is a useful agent for stabilizing folded states of proteins (Timasheff, 1993).

Recent advances in NMR and labeling techniques have permitted the characterization of the backbone dynamics of a variety of folded proteins. To date, however, considerably less is known about the dynamics of the unfolded state. Experiments have principally focused on the establishment of global characteristics of the unfolded form, including helical content and the effective radius of gyration (Shortle, 1993). Measurement of ^{15}N relaxation parameters permits the dynamics of the unfolded state to be examined on a per-residue basis and enables characterization of the extent to which the motional properties of unfolded and folded states of a protein differ. From measurements of ^{15}N T_1 and T_2 relaxation times, Fesik and co-workers (Logan et al., 1994) observed that in 6.3 M urea the unfolded state of FKBP exhibits greater conformational freedom at the N- and C-termini. While this observation parallels the results of many relaxation studies of domains of folded proteins, the terminal regions of folded FKBP do not show noticeable increases in T_1 and T_2 values (Cheng et al., 1993, Cheng et al., 1994). In another NMR study of a denatured protein, residual structure in the 434 repressor protein was described (Neri et al., 1992), indicating that at least in certain regions of this molecule large amplitude motion must be constrained.

This paper describes the characterization of the backbone dynamics and kinetics of the folding transition of an equilibrium mixture of folded and unfolded forms of the drkN SH3 domain, using NMR experiments specifically designed to determine relaxation parameters in the presence of exchange. Relaxation parameters of a particular backbone nitrogen atom are related to the spectral density function of the associated amide bond vector, which in turn reports on motions of the protein backbone. The most common approach to the extraction of dynamics information from relaxation parameters employs the model-free spectral density function described by Lipari and Szabo (1982a,b). While this method is very powerful for extracting useful dynamical parameters from relaxation data of folded proteins, its applicability to an unfolded protein, which is unlikely to tumble isotropically in solution, is less certain. For this reason we have chosen to present our data primarily in terms of the values of the spectral densities themselves. The approach that we adopt is thus similar in principle to the "spectral density mapping" technique described by Peng and Wagner (1992a,b), although there are some significant differences between the two approaches, as indicated below.

MATERIALS AND METHODS

NMR Studies. An ^{15}N-enriched sample of the N-terminal SH3 domain of drk was prepared as described previously (Zhang et al., 1994). All spectra were acquired using a 1 mM sample of the SH3 domain, 50 mM sodium phosphate, pH 6.0, 90% H_2O, and 10% D_2O.

The pulse sequences used to determine ^{15}N T_2 values and $^1H-^{15}N$ steady-state NOEs are shown in Figure 2, panels a and b, respectively. The pulse scheme used for the determination of longitudinal relaxation rates has been described in detail elsewhere (Farrow et al., 1994a). An important component of the pulse sequences used to determine ^{15}N relaxation rates is that the ^{15}N chemical shift labeling period occurs prior to the relaxation period T. Labeling the magnetization prior to the relaxation period permits discrimination between nuclei that undergo exchange between the folded and unfolded states during the relaxation period T and those that do not. The resultant $^1H-^{15}N$ correlation spectra generated from application of the sequence shown in Figure 2a, or from the corresponding T_1 scheme described previously, consist of four peaks for each backbone amide: a pair of "auto" peaks for which the ^{15}N and NH chemical shifts correspond to the same state and a pair of "exchange" cross peaks for which the chemical shifts correspond to different states resulting from a transfer of magnetization during the period T. While the auto peaks would be obtained in any type of heteronuclear correlation experiment, the cross peaks are observed only if the evolution period t_1 precedes the relaxation period T. An enhanced sensitivity approach (Cavanagh et al., 1991; Palmer et al., 1991a) may not be employed in the present case for the following reasons. The nature of the T_1 experiment prevents the preservation of both the sine and cosine components of the magnetization during the period T, while in the T_2 experiment imperfections in the ^{15}N 180° pulses during the CPMG pulse train will affect the sine and cosine components of the magnetization differently, leading to potential errors in the measured T_2 values. In principle, steady-state $^1H-^{15}N$ NOE values could be measured using the pulsed field gradient enhanced sensitivity scheme that we have presented previously (Farrow et al., 1994b); however, this approach was not employed in the study described here.

It is particularly important that care be taken to minimize saturation of water when performing a comparative study of folded and unfolded states in which amide proton exchange with bulk solvent is likely to be significantly higher in the unfolded form. Thus, the pulse sequences employ

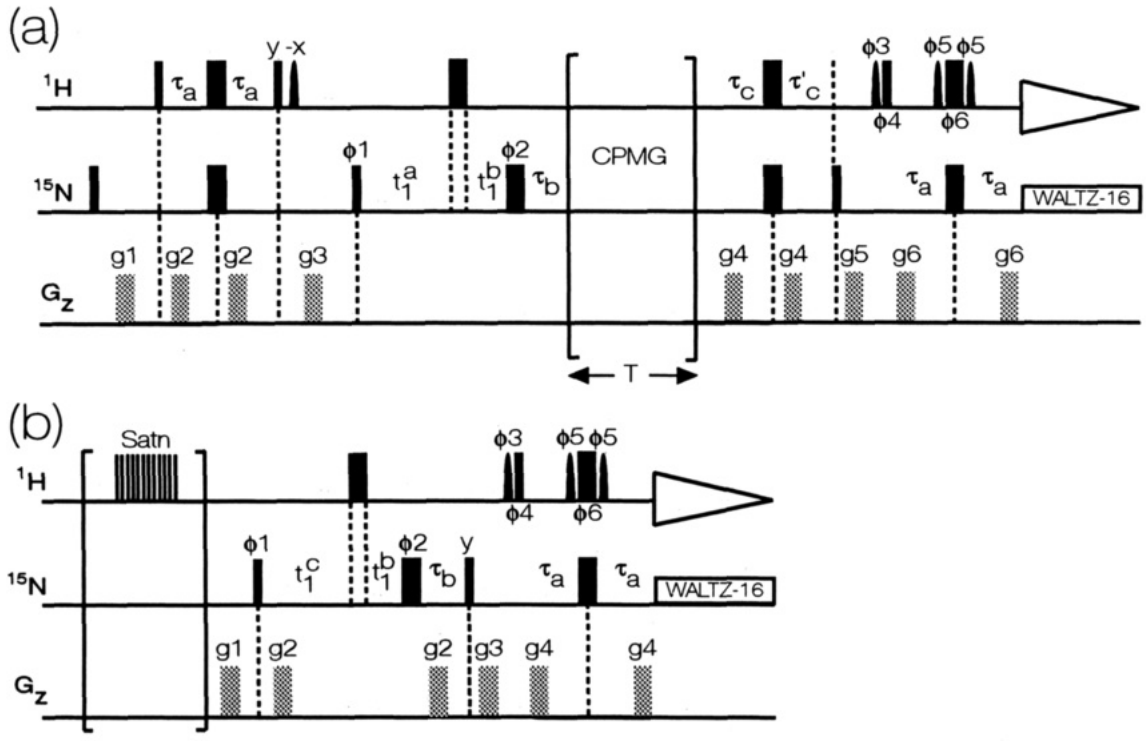

FIGURE 2: Pulse sequences used for the measurement of (a) ^{15}N T_2 values and (b) ^{1}H−^{15}N steady-state NOEs in the exchanging SH3 system considered in this paper. Narrow and wide pulses indicate 90° and 180° pulses, respectively. Water-selective pulses (all 90° pulses) are denoted by the shaped pulses in the figure. Unless indicated otherwise, all pulses are applied along the x axis. In both experiments the value of τ_a is set to 2.25 ms ($<1/(4J_{NH})$), τ_c is set to 2.75 ms ($1/(4J_{NH})$), $t_1^a = \tau_c + t_1/2 - (2/\pi)$(pwn) − 2(pw), $t_1^b = t_1/2 - n\zeta$, $t_1^c = \tau_c + t_1/2 - 2$(pw), $\tau_b = \tau_c - n\zeta$, $\tau'_c = \tau_c - (2/\pi)$(pwn), and $\zeta = \tau_c/(N - 1)$, where N is the number of complex points in the nitrogen dimension, $n = 0, 1, 2, ..., (N - 1)$, and pw and pwn are the widths of the ^{1}H and ^{15}N 90° pulses, respectively. The value of t_1 is set to n/SW1, where SW1 is the spectral width in F_1 (Grzesiek & Bax, 1993; Logan et al., 1993). WALTZ-16 decoupling (Shaka et al., 1983) of ^{15}N is applied during acquisition using a 1 kHz field. The water-selective 90° pulses are applied with the carrier on the water resonance as 125 Hz rectangular pulses (2 ms). A relaxation delay of 1 s is used in the T_2 experiment. The phase cycling in both the T_2 and NOE experiments is as follows: $\phi_1 = x$; $\phi_2 = 4(x), 4(y), 4(-x), 4(-y)$; $\phi_3 = 2(x), 2(-x)$; $\phi_4 = 2(x), 2(-x)$; $\phi_5 = x, -x$; $\phi_6 = -x, x$; and rec = $2(x), 4(-x), 2(x)$. Quadrature in F_1 is achieved via States−TPPI of ϕ_1 (Marion et al., 1989). Gradient durations and levels in the T_2 experiment are as follows: $g_1 = 1$ ms, 5 G cm^{-1}; $g_2 = 0.5$ ms, 4 G cm^{-1}; $g_3 = 1$ ms, 15 G cm^{-1}; $g_4 = 0.5$ ms, 8 G cm^{-1}; $g_5 = 1$ ms, −20 G cm^{-1}; $g_6 = 0.125$ ms, 25 G cm^{-1}. The CPMG pulse train used in the T_2 pulse sequence has been described in detail previously (see Figure 10b, Farrow et al., 1994b). Gradient levels and durations in the NOE experiment are as follows: $g_1 = 1$ ms, 5 G cm^{-1}; $g_2 = 0.1$ ms, 20 G cm^{-1}; $g_3 = 0.5$ ms, 3 G cm^{-1}; $g_4 = 0.13$ ms, 25 G cm^{-1}.

selective pulses in order to minimize water saturation and to ensure that water magnetization is returned to the $+z$ axis immediately prior to the detection period (Grzesiek & Bax, 1993; Kay et al., 1994; Stonehouse et al., 1994). One potential source of water saturation arises from the application of ^{1}H 180° pulses every several milliseconds during the period T of either the T_1 or T_2 pulse schemes. While these pulses are required to suppress cross-correlation effects between ^{1}H−^{15}N dipolar and ^{15}N chemical shift anisotropy relaxation mechanisms (Boyd et al., 1990; Palmer et al., 1992; Kay et al., 1992), they result in the water signal becoming increasingly attenuated as a function of T. This leads to a significant decrease in the intensity of cross peaks originating from labile protons and, in turn, to an increase in the apparent ^{15}N relaxation rates. In order to minimize this problem in the T_1 experiment, the ^{1}H 180° pulses applied during the period T have a cosine-modulated shape (Smallcombe, 1993) which produces a broad excitation null on resonance (i.e., at the water frequency). Similarly, during the CPMG period of the T_2 scheme, the ^{1}H 180° pulses are applied as pairs of $+x$ and $-x$ pulses such that the water experiences no net rotation during this period (Farrow et al., 1994b).

T_1, T_2 and ^{1}H−^{15}N NOE experiments were recorded at 14 °C on a Varian Unity 500 MHz spectrometer equipped with a triple resonance pulsed field gradient probe with an actively shielded z-gradient and a gradient amplifier unit. An additional T_2 experiment was recorded under identical measuring conditions on a Varian Unity Plus 600 MHz spectrometer. T_1 experiments were performed with 10 relaxation delays T: $T = 0.011$, 0.044, 0.078, 0.100, 0.155, 0.233 (×2), 0.322, 0.433, 0.588, 0.843 s. T_2 experiments were recorded with 8 relaxation delays T: $T = 0.016$, 0.033, 0.049, 0.066, 0.082, 0.099, 0.115, 0.148 s. A recycle delay of 1 s was employed when recording the T_1 and T_2 experiments. The equilibrium constants of the drkN SH3 system were calculated using the relative concentrations of the folded and unfolded states determined from a "fully relaxed" T_1 spectrum recorded with $T = 0$ and a recycle delay of 5 s between experiments. Note that the measured T_1 of water in this sample at 14 °C is 1.4 s. Steady-state ^{1}H−^{15}N NOE values were determined from spectra recorded in the presence and absence of proton saturation. Saturation was achieved by the application of ^{1}H 120° pulses every 5 ms (Markley et al., 1971). NOE spectra recorded with proton saturation utilized a 2 s relaxation delay followed by a 3 s period of saturation while spectra recorded in the absence of proton saturation employed a relaxation delay of 5 s. Two pairs of NOE spectra were recorded.

Data Processing and Analysis. All 500 MHz spectra were recorded as 160 × 512 complex matrices with 32 scans per t_1 point and were acquired with spectral widths of 8000 and

1500 Hz in the ^1H and ^{15}N dimensions, respectively. The T_2 spectra recorded at 600 MHz were acquired as 128 × 608 complex matrices with 16 scans per t_1 point and with spectral widths of 10 000 and 1800 Hz in the ^1H and ^{15}N dimensions, respectively. Lorentzian-to-Gaussian apodization functions were applied in both dimensions prior to Fourier transformation. All data were processed using nmrPipe software (Delaglio, 1993), and peak intensities were characterized as volumes using surface fitting routines in the nmrPipe software.

In a previous publication (Farrow et al., 1994a), we have presented equations that describe the evolution of longitudinal magnetization for a system undergoing exchange between two states. These expressions result from solution of the Bloch equations including the effects of chemical exchange (Hahn & Maxwell, 1952; Gutowsky & Saika, 1953; McConnell, 1958; Hull & Sykes, 1975) and for completeness are repeated here. The intensities of the folded and unfolded auto peaks are denoted by I_{ff} and I_{uu}, respectively, while intensities of the cross peaks arising from the exchange of magnetization from the folded (unfolded) to the unfolded (folded) state are denoted by I_{fu} (I_{uf}). The time evolution of the intensities of these four cross peaks in T_1 spectra is given by:

$$I_{ff}(T) = I_f(0)\{-(\lambda_2 - a_{11})\exp(-\lambda_1 T) + (\lambda_1 - a_{11})\exp(-\lambda_2 T)\}/(\lambda_1 - \lambda_2) \quad (1)$$

$$I_{uu}(T) = I_u(0)\{-(\lambda_2 - a_{22})\exp(-\lambda_1 T) + (\lambda_1 - a_{22})\exp(-\lambda_2 T)\}/(\lambda_1 - \lambda_2) \quad (2)$$

$$I_{fu}(T) = I_f(0)\{a_{21}\exp(-\lambda_1 T) - a_{21}\exp(-\lambda_2 T)\}/(\lambda_1 - \lambda_2) \quad (3)$$

$$I_{uf}(T) = I_u(0)\{a_{12}\exp(-\lambda_1 T) - a_{12}\exp(-\lambda_2 T)\}/(\lambda_1 - \lambda_2) \quad (4)$$

where $\lambda_{1,2} = (1/2)\{(a_{11} + a_{22}) \pm [(a_{11} - a_{22})^2 + 4k_{fu}k_{uf}]^{1/2}\}$, $a_{11} = 1/T_{1,f} + k_{fu}$, $a_{12} = -k_{uf}$, $a_{21} = -k_{fu}$, $a_{22} = 1/T_{1,u} + k_{uf}$. The longitudinal relaxation times of magnetization in the folded and unfolded states are denoted by $T_{1,f}$ and $T_{1,u}$, respectively, and k_{fu} and k_{uf} are the exchange rates from the folded to the unfolded state and from the unfolded to the folded state, respectively. The amount of longitudinal magnetization in the folded and unfolded states at the start of the mixing period T is given by $I_f(0)$ and $I_u(0)$, respectively. Note that magnetization is stored alternatively along the $+z$ and $-z$ axes such that the resultant decay is independent of $I_f(\infty)$ and $I_u(\infty)$ (Sklenar et al., 1987).

As indicated in Figure 2a, a CPMG pulse train was employed in the pulse sequence used for the determination of transverse relaxation rates. Numerical simulations were performed to examine the effects of chemical exchange on the measured transverse relaxation times. Simulations employed exchange rates and chemical shift differences typical of those seen in drkN SH3 ($\Delta\upsilon \leq 300$ Hz, $k_{fu} \approx k_{uf} \approx 0.5$ s^{-1}) and a 900 μs spacing between successive ^{15}N 180° pulses in the CPMG sequence. The decay of magnetization corresponding to the auto peaks was found to be independent of exchange for values of k_{fu}, k_{uf}, and $\Delta\upsilon$ relevant to the drkN SH3 system considered here. Therefore, the time evolution of such peaks is correctly described by expressions of the form given in eqs 1 and 2 when the longitudinal relaxation rates in the terms a_{11} and a_{22} are replaced by the corresponding transverse relaxation rates. In contrast, the effects of chemical exchange significantly attenuate the buildup of exchange cross peaks, and therefore the time evolution of these peaks in the T_2 experiment is not correctly described by expressions similar to those of eqs 3 and 4. Because the evolution of the exchange cross peaks in T_2 spectra is dependent on both the chemical shift differences of the exchanging states and the exchange rates, and since such peaks have inherently low sensitivity, the time dependence of these peaks was not included in the analysis described below.

Peak volumes in the NOE experiments are also affected by exchange between the two states. It is straightforward to show that the ratio of the peak intensities corresponding to ^{15}N magnetization of the folded state in the presence and absence of proton saturation, I_{fz}(sat) and I_{fz}(unsat), respectively, including the effects of chemical exchange, is given by:

$$\frac{I_{fz}(\text{sat})}{I_{fz}(\text{unsat})} = \frac{\{1/T_{1,f} + \sigma_f(\gamma_H/\gamma_N) + \alpha[1/T_{1,u} + \sigma_u(\gamma_H/\gamma_N)]\}}{(1/T_{1,f} + k_{fu} - \alpha k_{uf})} \quad (5)$$

where $\alpha = k_{fu}/(1/T_{1,u} + k_{uf})$, γ_i is the gyromagnetic ratio of spin i, and σ_f and σ_u are the $^1H-^{15}N$ cross-relaxation rates in the folded and unfolded states, respectively. A similar expression holds for the ratio of ^{15}N magnetization in the unfolded state in the presence and absence of ^1H saturation and can be obtained directly by interchanging the labels f and u in eq 5.

Equations 1−5 indicate that the evolution of magnetization in an exchanging system is complicated by the exchange process itself. For example, the intensity of the ff cross peak in the T_1 experiment, $I_{ff}(T)$, is a function of both $T_{1,f}$ and $T_{1,u}$, as well as the exchange rate between the two forms. Application of the equations described above to fit the experimental data allows the relaxation parameters of the folded and unfolded states to be obtained.

Extraction of information about the dynamics of a protein from ^{15}N relaxation rates and NOE measurements is possible because these parameters are directly related to the spectral density function describing the contributions of different frequencies to the motion of the individual amide bond vectors. The expressions given by Abragam (1961) relate the longitudinal and transverse relaxation rates and the steady-state NOE to the spectral density function at 5 distinct frequencies: 0, ω_N, $\omega_H + \omega_N$, ω_H, and $\omega_H - \omega_N$. In the absence of any assumption about the form of the spectral density function, the three experiments described above do not provide enough information to enable direct determination of the spectral density function at all 5 frequencies. This information may be obtained from the measurement of additional relaxation parameters, as described in the spectral density mapping approach of Peng and Wagner (1992a,b). Alternatively, assumption of a specific form for the spectral density function, for example, using the model-free approach of Lipari and Szabo (1982a,b) with parameters τ_m, S^2, and τ_e (see below), permits the determination of the spectral density function from measurements of T_1, T_2, and the steady-state NOE. The approach adopted in the study described here is similar to the spectral density mapping method of Peng and Wagner (1992a) with an additional simplifying

assumption that the spectral density function has a similar magnitude at the three frequencies $\omega_H + \omega_N$, ω_H, and $\omega_H - \omega_N$. Therefore, $J(\omega_H+\omega_N)$, $J(\omega_H)$, and $J(\omega_H-\omega_N)$ may be replaced with a single spectral density value, $J(\omega_h)$. In their study of the 8 kDa protein, eglin *c*, Peng and Wagner determined that the 3 high frequency terms of the backbone amide spectral density function were of similar magnitude and that they were very much smaller than either the $J(0)$ or $J(\omega_N)$ terms (Peng & Wagner, 1992b). Assuming a model-free functional form (Lipari & Szabo, 1982a,b) for $J(\omega)$, a negligible contribution to relaxation from internal motions, and an overall correlation time of 5 ns, the three highest frequency spectral density functions $J(\omega_H+\omega_N)$, $J(\omega_H)$, and $J(\omega_H-\omega_N)$ are approximately equal and are only 0.5%, 0.4%, and 0.3% the size of the $J(0)$ component, respectively. Thus, it is a reasonable approximation to collect the contributions of the three highest frequency spectral densities under a single term, $J(\omega_h)$. With this assumption, the relationships between the spectral density functions, the relaxation parameters, and the cross-relaxation rates for the folded and unfolded states become:

$$1/T_{1,f/u} = (d^2/4)[3J_{f/u}(\omega_N) + 7J_{f/u}(\omega_h)] + c^2J_{f/u}(\omega_N) \quad (6)$$

$$1/T_{2,f/u} = (d^2/8)[4J_{f/u}(0) + 3J_{f/u}(\omega_N) + 13J_{f/u}(\omega_h)] + (c^2/6)[4J_{f/u}(0) + 3J_{f/u}(\omega_N)] \quad (7)$$

$$NOE_{f/u} = 1 + (d^2/4)(\gamma_H/\gamma_N)[5J_{f/u}(\omega_h)]T_{1,f/u} \quad (8)$$

$$\sigma_{f/u} = (d^2/4)[5J_{f/u}(\omega_h)] \quad (9)$$

where $d = \mu_0 h\gamma_N\gamma_H/(8\pi^2\langle r_{NH}\rangle^3)$, $c = (\omega_N/\sqrt{3})(\sigma_{||} - \sigma_\perp)$, μ_0 is the permeability of free space, h is Planck's constant, r_{NH} is the amide bond length, $\sigma_{||}$ and $\sigma_\perp$ are the parallel and perpendicular components of the chemical shift anisotropy tensor ($\sigma_{||} - \sigma_\perp = -160$ ppm for a backbone amide (Hiyama et al., 1988) and -89.6 ppm for the side-chain indole nitrogen of tryptophan (Cross & Opella, 1983)), and the subscripts f and u refer to the folded and unfolded states, respectively. Note that, in the case of isotropic motion using the Lipari–Szabo formalism (1982a,b), $J(\omega)$ is defined:

$$J(\omega) = (2/5)\{S^2\tau_m/[1 + (\omega\tau_m)^2] + (1 - S^2)\tau/[1 + (\omega\tau)^2]\} \quad (10)$$

where τ_m is the overall correlation time, S^2 is the generalized order parameter, τ_e is the correlation time for internal motions, and $\tau^{-1} = \tau_m^{-1} + \tau_e^{-1}$.

Equations 6–9 permit the values of the spectral density functions to be used as fitting parameters when modeling the experimental data. The values of the spectral density functions and exchange rates were extracted directly by simultaneously fitting (i) the decay/buildup curves of the auto and cross peaks from the T_1 spectra, (ii) the decay curves of the auto peaks from the T_2 spectra, and (iii) the $^1H-^{15}N$ steady-state NOE values, using the expressions given in eqs 1–9. In total, 11 parameters were required to fit the data: the three spectral densities, $J(0)$, $J(\omega_N)$, and $J(\omega_h)$, for both the folded and unfolded states; the initial intensities of the folded and unfolded magnetization in the T_1 and T_2 experiments; and the exchange rate k_{fu}. The exchange rate k_{uf} was calculated using the relationship $k_{uf} = K_{eq}k_{fu}$, with K_{eq} determined from a fully relaxed spectrum recorded using the T_1 sequence with $T = 0$. Initial estimates of the spectral density function search parameters were derived using eqs 6–9 in conjunction with estimates of $T_{1,f}$, $T_{1,u}$, $T_{2,f}$, and $T_{2,u}$ obtained from the initial slopes of the auto peak decay curves in the T_1 and T_2 experiments and estimates of the cross-relaxation rates from steady-state $^1H-^{15}N$ NOE spectra. None of these estimates provide a direct measurement of the relaxation parameters of either the folded or unfolded states since the measured parameters contain contributions from both forms. Nevertheless, the estimates obtained using this approach were sufficient to produce rapid convergence of the fitting parameters. The optimization procedure employed a χ^2 goodness of fit parameter which contained contributions from all 6 measured buildup/decay curves and the measured steady-state NOE values of the folded and unfolded forms of the molecule. In theory, a maximum of 58 data points were available for each residue; however, ill-determined initial values of exchange cross peak intensities and cross peak overlap typically reduced the number of available data points to approximately 50. All data analysis programs were written in C and utilized the Levenberg–Marquardt minimization algorithm provided in the IMSL subroutine libraries (IMSL, Houston, TX). Errors in the fitted parameters were determined using a Monte Carlo procedure (Kamath & Shriver, 1989; Palmer et al., 1991b).

While the spectral density mapping approach described above yields values of the spectral density functions directly, a more intuitive appreciation of the dynamics of the protein may be gained by application of the model-free spectral density function approach of Lipari and Szabo (1982a,b). However, it must be stressed that parameters for the unfolded state of drkN SH3 derived using this approach should be treated qualitatively since it is unlikely that the dynamics of an unfolded state can be modeled accurately using a spectral density function which assumes isotropic molecular tumbling and which has only a single correlation time to describe internal dynamics. In this study, a methodology similar to that applied previously by ourselves and others in order to determine values of the model-free spectral density function parameters has been adopted (Kördel et al., 1992; Stone et al., 1993; Akke et al., 1993; Farrow et al., 1994b). Briefly, the simplest form of the model-free spectral density function describes the motion of the NH bond vector in terms of three parameters, τ_m, S^2, and τ_e. A grid search was performed to determine the optimum overall correlation time (τ_m) for both the folded and unfolded states of the molecule, fitting each residue within the molecule using a model-free spectral density function containing the free parameters S^2 and τ_e. Once the optimum values of the overall correlation times had been determined, a Monte Carlo analysis was performed to determine the uncertainties associated with the fitting parameters, S^2 and τ_e, of each residue based on the errors in the measured relaxation parameters.

RESULTS AND DISCUSSION

Equilibrium Constants. ^{15}N and ^1H NMR resonance assignments of the backbone amides of the folded and unfolded states of the drkN SH3 domain in this exchanging system have been reported previously (Zhang et al., 1994). The drkN SH3 domain contains 59 residues, one of which is a proline. Fifty residues of the folded state and 17 residues of the unfolded state have well-resolved backbone amide cross peaks in the HSQC spectrum of the equilibrium system. The limited number of resolved peaks in the unfolded state

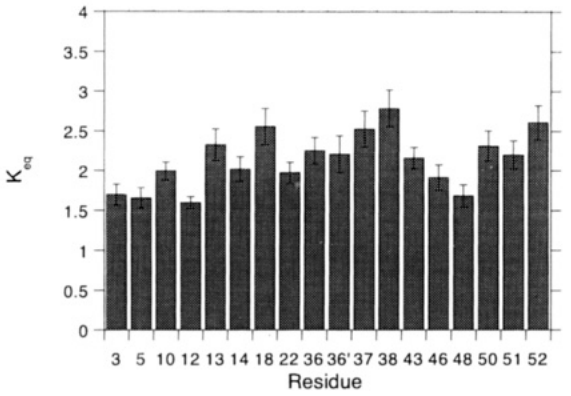

FIGURE 3: Plot of equilibrium constants, K_{eq}, for the 17 residues resolved in both forms of the drkN SH3 domain. The equilibrium constant derived from the side-chain (^{15}N,NH) spin pair of the indole ring of Trp 36 is also shown and is denoted 36'. Values of K_{eq} were determined from the volume ratios of peaks corresponding to folded and unfolded states in a fully relaxed spectrum (folded/unfolded).

is due to the poor chemical shift dispersion in the NH dimension frequently observed in spectra of unfolded proteins. In addition, the side-chain NH of Trp 36 is resolved in both the folded and unfolded forms. Equilibrium constants, K_{eq}, for the folding transition at 14 °C, pH 6, 50 mM sodium phosphate, were calculated for 17 residues and are plotted in Figure 3. The mean value of K_{eq} (±one standard deviation) was determined to be 2.13 ± 0.36, with an uncertainty in individual values of approximately 8% estimated from errors in peak heights and peak widths. Therefore, the experimental uncertainty does not account for the variations in the measured K_{eq} associated with different residues in the SH3 domain. The largest value of K_{eq} is a factor of 1.7 greater than the smallest. This range of variation in K_{eq} corresponds to a small difference in $\Delta G \leq 1.33$ kJ mol^{-1} (0.32 kcal mol^{-1}), indicating that the observed variations in K_{eq} correspond to small differences in the stability of the folded structure as a function of residue. The values of K_{eq} do not appear to correlate in a significant manner with either the secondary or tertiary structure of the folded SH3 domain. Additionally, no correlation is observed between residues having higher values of K_{eq} and those residues exhibiting weak sequential NH NOEs in the unfolded state. It is interesting to note that variations in the equilibrium constants of four His CϵH resonances have been described previously in association with the pH-induced folding transition of ribonuclease A (Benz & Roberts, 1975).

Studies of the folding transition of the SH3 domain of spectrin, using both fluorescence spectroscopy and circular dichroism to follow the kinetics of unfolding and refolding at pH 3.5, demonstrate that the folding transition for this SH3 domain is correctly described by a two-state approximation (Viguera et al., 1994). In contrast to the results obtained on the drkN SH3 domain, the two-state model predicts a single equilibrium constant for all residues. It should be noted that, unlike the NMR approach described here, circular dichroism and fluorescence studies cannot monitor transitions at the level of each residue in a protein. In the case of the fluorescence studies of the spectrin SH3 domain, for example, two tryptophan residues in the molecule report on the transition, while the circular dichroism studies are based on contributions from all residues. Data from our study were fit to a model that assumes that each residue undergoes a two-state transition, and the rate constants describing the folding and unfolding transition were permitted to vary on a per-residue basis with the constraint that their ratios equalled the measured equilibrium constant at each site. However, the model does not assume that the folding of the protein as a whole is cooperative. Preliminary data collected at 3 °C, where exchange is too slow to affect measured relaxation rates, show variations in relaxation parameters similar to those observed at 14 °C, suggesting that the model employed to fit the results at 14 °C is appropriate. Thermodynamic studies are planned to establish definitively whether or not the folding transition of the drkN SH3 domain can be described as a two-state cooperative process.

Relaxation Parameters and Exchange Rates. Examples of the spectra from the T_1 data series are shown in Figure 4. To illustrate the development of the exchange cross peaks, two time points are presented: the initial time point, $T = 0.011$ s, and a later time point, $T = 0.322$ s, in which the exchange cross peaks are clearly seen. As discussed above, extraction of spectral density functions requires fitting (a) the decay curves of both auto peaks in the T_1 and T_2 experiments, (b) the buildup/decay curves of at least one (preferably both) cross peak in the T_1 experiment, and (c) the ^{1}H$-^{15}$N steady-state NOEs of both the folded and unfolded species. The fact that both auto and exchange cross peaks are required for data analysis imposes significant limitations on the number of residues that can be fitted. Sufficient data were available for the characterization of only 12 backbone amides and the side-chain indole nitrogen of Trp 36. Examples of the fits achieved for several of the T_1 curves are shown in Figure 5.

T_1, T_2, and NOE values of both the folded and unfolded states, extracted using the previously described fitting procedure, are presented in Figure 6. The error bars in the figure indicate the estimated uncertainties (one standard deviation) of the parameters as determined by Monte Carlo methods (Kamath & Shriver, 1989; Palmer et al., 1991b). Generally, errors in the relaxation parameters associated with the unfolded state are higher than those of the folded state due to the lower signal-to-noise ratio of cross peaks of the unfolded form. Note that the T_1, T_2, and NOE values determined by this approach relate solely to the folded or unfolded states. That is, the effects of exchange between the two states have been removed, and the values are, in principle, identical to those that would be determined in a nonexchanging system. Figure 6a shows that the T_1 values of the folded state of the SH3 domain are relatively constant throughout the molecule. In contrast, in the unfolded state, considerable variation of T_1 values is observed, with increasing values toward the N-terminus of the molecule. While the measured T_1 values of residues in the folded state are in all cases lower than those of the unfolded form, for many residues the absolute difference in the longitudinal relaxation times of the two states is small.

The T_2 values of residues in the folded state are also relatively constant throughout the molecule. Again, significant variations are observed in the T_2 values of residues in the unfolded state (Figure 6b). As with the T_1 values, in all cases the T_2 values of residues in the folded state are lower than those of the unfolded state. Backbone T_2 values of the folded and unfolded state are most similar for residues toward the middle of the sequence, Thr 22, Trp 36, and Arg 38. Above average mobility of the N-terminal region of the unfolded state is indicated by the high T_2 values for residues Ala 3 and Ala 5.

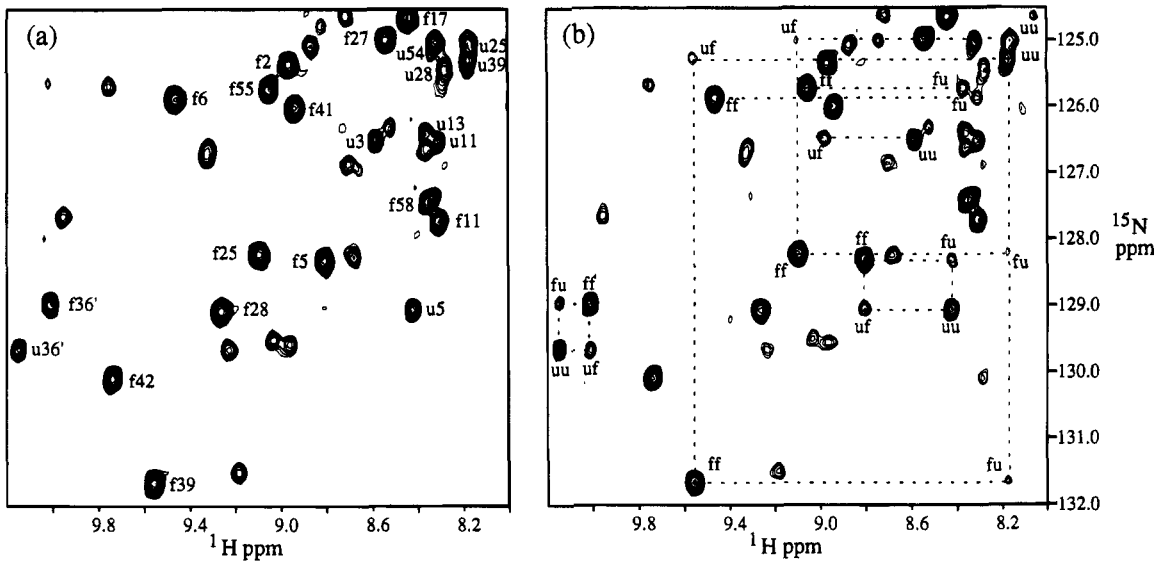

FIGURE 4: Representative regions of the T_1 2D $^1H-^{15}N$ correlation spectra at (a) $T = 0.011$ s and (b) $T = 0.322$ s. Cross peaks are labeled in (a) according to their amino acid sequence number, with cross peaks of residues in the folded and unfolded states identified by the prefixes "f" and "u", respectively. The cross peak corresponding to the side-chain NH of Trp 36 is denoted 36'. The cross peaks in (b) are labeled according to the convention described in the text. Auto and exchange cross peaks of each residue are connected by dashed lines.

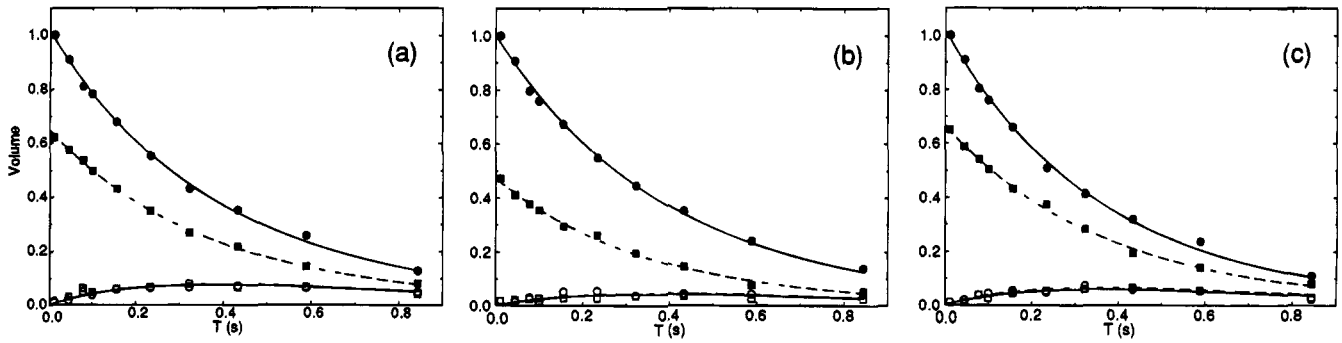

FIGURE 5: Illustrations of the fitted curves obtained from the T_1 data of (a) Gly 12, (b) Trp 36 (backbone), and (c) Ile 48, representing the best, worst, and average fits to the experimental data, respectively. Solid symbols indicate data derived from the auto peaks, ff and uu; open symbols indicate data from the exchange cross peaks, fu and uf. The intensities of all peaks are normalized such that the intensity of the ff peak at the earliest time point is set to 1.0. Data points marked with circles indicate magnetization arising from the folded state, ff and fu, whereas squares indicate magnetization originating in the unfolded state, uu and uf.

The $^1H-^{15}N$ NOEs of all residues in the unfolded state were less than in the folded state (Figure 6c). Paralleling observations for the relaxation times, relatively little variation is observed in the NOEs of residues in the folded state, whereas the NOEs of residues in the unfolded state show considerable variation, ranging from 0.39 to −1.1. The variation in the NOE values of the unfolded state is correlated with the observed T_2 values of that state. For example, the increase in NOE values from Ala 3 to Thr 22 parallels the decrease in the T_2 values observed for these residues. Additionally, residues that have the largest backbone NOE values, Thr 22, Trp 36, and Arg 38, are also those residues with the smallest values of T_2. At the C-terminus, the correlation between the T_2 and NOE values is not as striking, the NOE values suggesting steadily increasing mobility of this region between residues Gly 43 and Ser 50.

Comparison of the T_1, T_2, and NOE data of the folded and unfolded forms reveals that, of the residues characterized, Thr 22, Trp 36, and Arg 38 have the most similar backbone ^{15}N relaxation parameters in the two states. In the folded state, residues Trp 36 and Arg 38 are in strand $\beta 5$ in the center of a three-strand β-sheet. In the unfolded state, these residues display NH_i-NH_{i+1} NOE connectivities. In contrast, residue Thr 22 is found in a turn in the folded state. While it is tempting to associate the similarity in relaxation parameters for residues Trp 36 and Arg 38 with the sequential NH NOEs observed in the unfolded state, it should be noted that other residues (e.g., Gly 43 and Gly 46) which also show NH NOEs have noticeably different values of the relaxation parameters in the two states.

T_1, T_2, and steady-state NOE measurements are available for 5 residues N-terminal of Thr 22. Significant differences between the relaxation parameters for the unfolded and folded states are observed for these residues. All three relaxation parameters indicate that this region exhibits greater mobility in the unfolded state. Of these 5 residues, Ala 3 and Ala 5 are in strand $\beta 1$, while Thr 12, Ala 13, and Asp 14 lie in the loop between strands $\beta 2$ and $\beta 3$.

The values of the exchange rate constants, k_{fu} and k_{uf}, extracted from the fitting procedure are shown in Figure 6d. The variations in the rates between residues exceed the calculated experimental uncertainties, indicated by the error bars in the figure. While it is difficult to draw conclusions concerning trends in the value of the exchange rates as a function of sequence, it is of interest to note that the average value of the rate constant k_{uf} (0.89 s^{-1}) is similar to the rate of formation (0.7−1.4 s^{-1}) of stable β-sheet structure in interleukin-1β (Varley et al., 1994) and is significantly slower

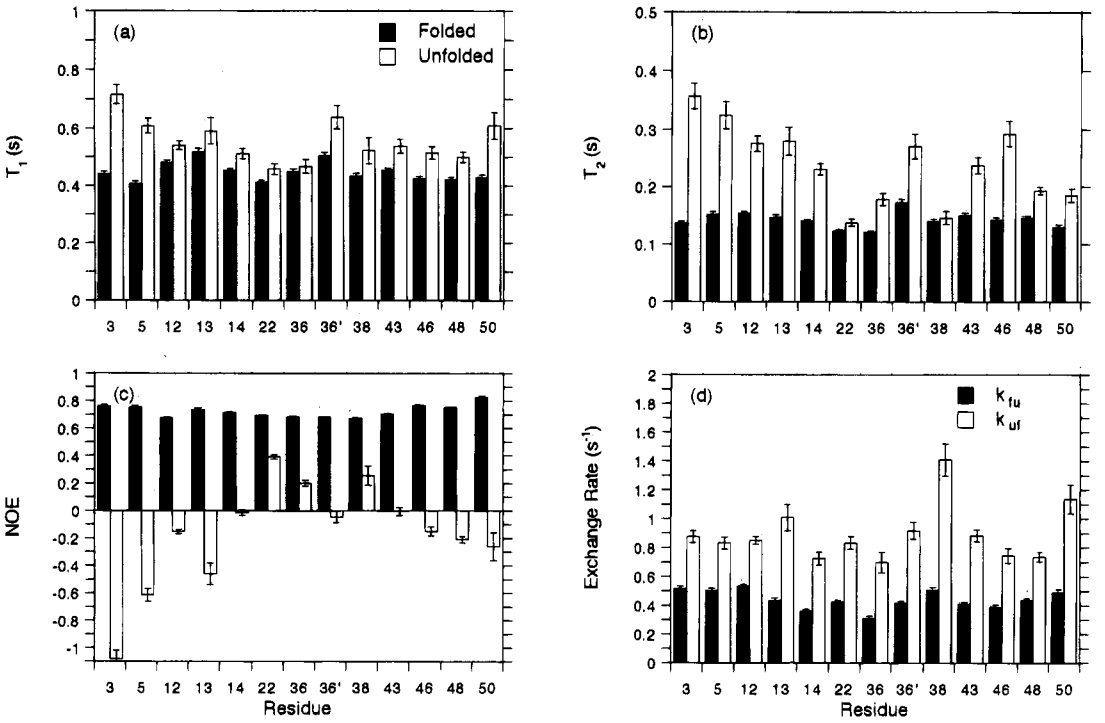

FIGURE 6: Plots of (a) T_1, (b) T_2, (c) NOE, and (d) the exchange rates k_{fu} and k_{uf} for the backbone amides of 12 residues and the indole NH of Trp 36 (denoted 36') of the drkN SH3 domain. All parameters were derived using the fitting procedure described in the text. In (a), (b), and (c), data pertaining to the folded state are indicated by the black bars; the white bars indicate values derived for the unfolded state. In (d), the black bars indicate the value of k_{fu}; the white bars indicate the value of k_{uf}.

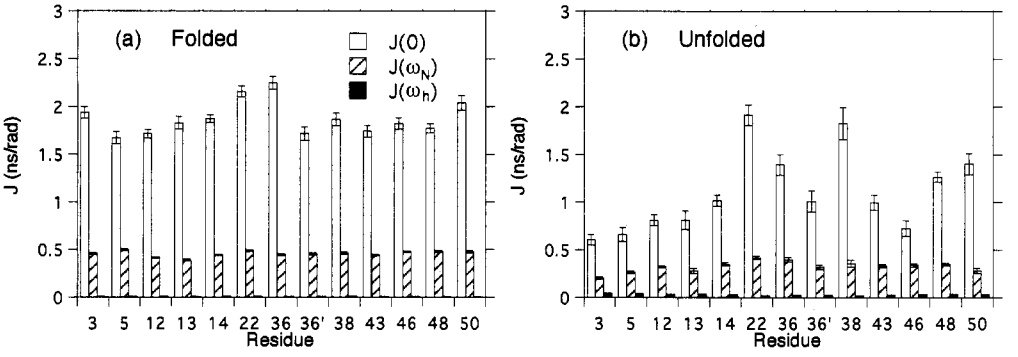

FIGURE 7: Calculated values of the spectral density functions of residues in (a) the folded and (b) the unfolded state. The white bars indicate values of $J(0)$, hatched bars $J(\omega_N)$, and the black bars $J(\omega_h)$. Note that, for the folded state, the values of $J(\omega_h)$ are just above the base line of the plot and the error bars for $J(\omega_h)$ are not visible at this scale. The cross peak corresponding to the side-chain NH of Trp 36 is denoted 36'.

than rates associated with the formation of α-helical structure (Gruenewald et al., 1979).

Spectral Density Functions. The values of the spectral density functions of the folded and unfolded states of the drkN SH3 domain are illustrated in Figure 7. As described above, the contributions of the high frequency terms of the spectral density function to the relaxation rates have been collected under the single term, $J(\omega_h)$. In both the folded and the unfolded forms of the drkN SH3 domain, the $J(0)$ terms of the spectral density function are larger than the $J(\omega_N)$ terms, which in turn are larger than the $J(\omega_h)$ terms. On average, the $J(0)$ and $J(\omega_N)$ terms of the unfolded form of the SH3 domain are a factor of 0.59 and 0.71 of those of the folded form, respectively. In contrast, the $J(\omega_h)$ terms of the unfolded form are approximately 3.4 times larger than those of the folded form. The magnitudes of $J(0)$, $J(\omega_N)$, and $J(\omega_h)$ are relatively uniform in the folded state of the drkN SH3 domain. This is not surprising given the uniformity of the relaxation parameters $T_{1,f}$, $T_{2,f}$, and NOE_f illustrated in Figure 6. In the unfolded state, the values of $J(0)$ and, to a lesser extent, $J(\omega_N)$ parallel the $T_{2,u}$ and NOE_u values illustrated in Figure 6. Thus larger values of $J(0)$ correspond to smaller T_2 values and increased steady-state $^1H-^{15}N$ NOEs. The backbone $J(0)$ values are largest for residues Thr 22, Trp 36, and Arg 38 (36' denotes the indole nitrogen of Trp 36) and, in fact, are of similar magnitude in both the folded and unfolded states. As described above, the degree of motion increases toward the N-terminus of the unfolded state and is reflected in a decrease in the magnitude of the terms $J(0)$ and $J(\omega_N)$.

A particularly important observation from the data presented in Figure 7 is that the relative sizes of the different components of the spectral density function all follow the relationship $J(0) > J(\omega_N) > J(\omega_h)$ for both the folded and unfolded forms of the domain. It is well-known that for molecules tumbling in the extreme narrowing regime, $\omega_L\tau_m \ll 1$, where τ_m is the overall correlation time and ω_L is the Larmor frequency, the value of $J(\omega)$ over a range of frequencies extending to $\approx 1/\tau_m$ is constant. Clearly, this is not the case for the unfolded state of the SH3 domain.

Rather, the unfolded state appears to adopt an ensemble of relatively compact structures, with an average radius of gyration that is not radically different from that in the folded state.

The analysis performed takes into account the effects of chemical exchange between the folded and unfolded states of the SH3 domain; it does not include the influence of conformational exchange between various populations within either the unfolded or the folded states themselves. This is particularly pertinent to the unfolded state, where the presence of $^3J_{HN\alpha}$ couplings of 6−7 Hz, as well as weak sequential CαH−NH and NH−NH NOEs from residues 35−47 and 52−54, suggests that a number of conformations are likely to be populated. Such conformational exchange processes will affect the transverse relaxation rates and give rise to elevated values of $J(0)$. In order to investigate the extent of these contributions in the drkN SH3 system, T_2 experiments have been performed at both 500 and 600 MHz. Rapid exchange between populations results in a contribution to the linewidth which scales as the square of the field strength. Therefore, measurements at different field strengths permit a straightforward evaluation of the extent that these processes contribute to measured T_2 values (Carrington & McLachlan, 1967). T_2 values for the 12 residues examined here were compared at 500 and 600 MHz. In the folded state, the T_2 values of 8 of the 12 backbone amide nitrogens were the same, within measurement error. Of the remaining 4 residues, T_2 values for Ala 5 and Gly 46 at 500 MHz were 1.08 and 1.12 times, respectively, the values at 600 MHz. The T_2 values of Trp 36 and Arg 38 at 500 MHz were 0.69 and 0.92, respectively, of the values at 600 MHz. Seven of the T_2 values measured for residues in the unfolded form at 500 and 600 MHz were the same within error. Of the remaining 5 residues, T_2 values for Ala 13 and Asp 14 measured at 500 MHz exceeded those at 600 MHz by factors of 1.07 and 1.05, respectively, while T_2 values for Ala 3, Arg 38, and Gly 46 at 500 MHz were 0.84, 0.83, and 0.74, respectively, of the values at 600 MHz. On the basis of these studies, it would seem that contributions to the transverse relaxation rates of the SH3 domain resulting from exchange between populations are relatively small and thus will not affect the validity of the conclusions presented in this paper.

While the measured values of the spectral density functions of the folded and unfolded states show some similar trends, there are a number of important differences. First, the fact that $J_f(0) > J_u(0)$ and $J_f(\omega_N) > J_u(\omega_N)$ demonstrates that residues in the unfolded state are more mobile. Second, significantly larger $J(\omega_h)$ values are observed in the unfolded SH3 domain. The latter observation is of some interest in light of results described by Peng and Wagner in their analysis of the spectral density functions of eglin *c* (1992b). These workers noted that the disordered N-terminal region of the protein and, to a lesser extent, the flexible proteinase binding loop exhibited above average values of the spectral density function at frequencies $\omega_H + \omega_N$, ω_H, and $\omega_H - \omega_N$. Therefore, the increased values of $J(\omega_h)$ seen in the unfolded state are consistent with its more extensive dynamic behavior. It is of interest to compare the relative sizes of the high and low frequency contributions to $J(\omega)$ in the SH3 system and in eglin *c* (Peng & Wagner, 1992b). In the folded form of the SH3 domain the average value of $J(0)$ is approximately 200 times the average value of $J(\omega_h)$ while in the unfolded form the average zero frequency component is 35 times the value at ω_h. Peng and Wagner found that, in the core of

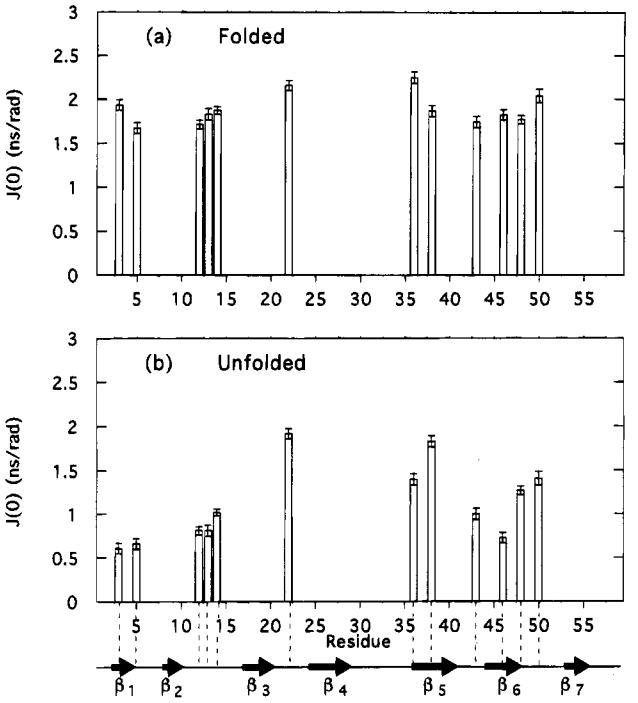

FIGURE 8: Values of $J(0)$ as a function of residue number for (a) the folded and (b) the unfolded states of drkN SH3. The schematic diagram at the base of the figure indicates the putative positions of the β-strands in the folded form of the domain based on homology modeling of the drkN SH3 domain using the recently determined structure of the N-terminal SH3 domain of grb2 (Wittekind et al., 1994). The values of $J(0)$ for the side-chain NH of Trp 36 are not shown in the figure.

eglin *c*, the $J(0)$ values were between 10 and 50 times the $J(\omega_h)$ values.

Comparison of the findings of our study to those of Peng and Wagner can lead to a better understanding of what the observed differences in the values of the spectral density function of the two states of the drkN SH3 domain imply about the dynamics of the unfolded state of the protein. The eglin *c* study revealed that the average values of $J(0)$ and $J(\omega_N)$ for the 8 amino-terminal residues and the residues associated with a flexible proteinase binding loop were significantly lower than values in the remainder of the protein. The average $J(0)$ value of the mobile binding loop in eglin *c* was approximately two-thirds the average value in the core of the protein, while the average $J(0)$ value of the 8 N-terminal residues was one-third the core value. By comparison, the average value of $J(0)$ of the unfolded form of SH3 is 0.59 times the value in the folded state, suggesting that picosecond to nanosecond motions of the unfolded state are more like those of the disordered, but constrained, proteinase binding loop than they are those of the highly disordered N-terminal region of eglin *c*.

Figure 8 illustrates the relationship between the observed values of $J(0)$ and the position of each residue in relation to the secondary structure of the folded state. The values of the spectral density function measured for the folded state of the SH3 domain do not show a large variation as a function of residue, indicating little correlation of motion with the secondary structure of the protein. In light of the results of Peng and Wagner it might have been expected that residues at the N-terminus, Ala 3 and Ala 5, and residues in loops, Asp 14, Gly 43, and Ser 50, would have decreased $J(0)$ or $J(\omega_N)$ terms. However, as illustrated in Figure 1, the folded drkN SH3 domain is extremely compact, having

no extended loops, and with the N-terminal residues closely associated with the core of the domain. In fact, based on homology to the structure of the N-terminal SH3 domain of grb2, the first 6 residues of the drkN SH3 domain are all expected to participate in hydrogen bonds with the rest of the protein. Clearly, the compact nature of the domain contributes significantly to the large and uniform spectral density values observed.

The observed stretch of weak NH_i-NH_{i+1} NOEs extending from Ser 34 to Leu 47 and from Tyr 52 to Glu 54 (Zhang & Forman-Kay, 1995) are of particular interest since they span a region of β-structure in the folded state including strands $\beta4$, $\beta5$, and $\beta6$. Initially, it was not clear whether the observation of these NOEs was due to the preferential sampling of the α-helical region of conformational space for these residues only, or whether residues in the entire molecule sample similar configurations but with dynamics such that similar NOEs are not observed for the other residues. Since the strength of homonuclear NOEs scales with $J(0)$ for molecules in the negative $^1H-^1H$ NOE regime ($\omega_H\tau_m \gg 1$), the spectral density values obtained in this study can address this question directly. Although Trp 36 and Arg 38 have above average $J(0)$ values, Gly 43 and Gly 46 do not. Moreover, Thr 22, which has the largest $J(0)$ of the 12 residues measured, does not show NH_i-NH_{i+1} or $C\alpha H_i-NH_{i+1}$ NOEs. Assuming that the $J(0)$ values are similar for the motion of $^{15}N-NH$ pairs and sequential NH−NH or CαH−NH pairs, the results of the present study imply that the observation of weak NH_i-NH_{i+1} NOEs in particular segments of the unfolded state of the drkN SH3 domain is a reflection of the propensity of these segments to preferentially sample certain regions of conformational space.

Model-Free Analysis. Overall molecular correlation times were determined as described in the Data Processing and Analysis section using a model which assumes isotropic molecular tumbling. An optimum value of τ_m of 5.5 ns was found for both forms of the domain when all residues were considered simultaneously in the fitting procedure. To examine this result further, optimal τ_m values were determined for each residue independently and the distributions of these values were examined. Mean values of τ_m of 5.6 and 5.8 ns were obtained for the folded and unfolded states with standard deviations of 0.4 and 1.6 ns, respectively. The large distribution of τ_m values within the unfolded SH3 domain suggests, not surprisingly, that the overall tumbling of the molecule in this state may not be accurately described by a single correlation time. Indeed, the difficulty in assigning a single overall correlation time to unfolded proteins has been described previously in the context of a partially folded form of BPTI (van Mierlo et al., 1993).

Despite the caveat regarding the characterization of the overall tumbling of the unfolded state by a single correlation time, model-free parameters S^2 and τ_e were nevertheless extracted for both forms of the SH3 domain using a value of $\tau_m = 5.5$ ns in each case. The results are reported in Table 1. As expected, the order parameters of the folded form of the protein are larger than those of the unfolded form. The average value of S^2 (backbone amides) of the folded SH3 domain was determined to be 0.85 and is similar to average values found for other folded proteins (Kay et al., 1989; Clore et al., 1990; Stone et al., 1992). The order parameters of the unfolded state, with an average value 0.48, are typical of values which have been determined previously for flexible loop regions of folded proteins (Clore et al., 1990; Akke et al., 1993). The distribution of order parameters in the two states is quite different. The range of S^2 values in the folded form is fairly small and like that in other folded proteins, while the distribution of values in the unfolded form is larger, suggesting a considerable range of disorder across the molecule. The backbone order parameters increase toward the center of the unfolded molecule, much like the $J(0)$ values, with residues Thr 22, Trp 36, and Arg 38 displaying the largest S^2 values. The internal correlation times, τ_e, determined for the folded form of the protein are typical of values found in other folded proteins, while τ_e values of the unfolded form are considerably larger and are similar to the value of 1 ns reported by van Mierlo et al. (1993) in their study of a folding intermediate of BPTI. It is interesting to note the parallel between the large values of τ_e ($\approx$1 ns) observed for the unfolded state and the 3−4-fold higher values of $J(\omega_h)$, which measure the extent of motions with frequencies on the order of 1 GHz, for the unfolded vs the folded SH3 domain. The increase in $J(\omega_h)$ values may well reflect the increase in nanosecond time scale motion observed in the unfolded state.

Table 1: Model-Free Parameters Derived for the Folded and Unfolded States of N-Terminal drk SH3[a]

	folded			unfolded		
residue	S^2	τ_e (ps)	χ^2	S^2	τ_e (ps)	χ^2
Ala 3	0.86 ± 0.01	4 ± 6	0.65	0.28 ± 0.06	186 ± 195	1.23
Ala 5	0.88 ± 0.02	10 ± 6	16.40	*b*	*b*	*b*
Thr 12	0.77 ± 0.01	34 ± 3	0.29	0.25 ± 0.05	1127 ± 121	29.95
Ala 13	0.77 ± 0.02	11 ± 5	8.29	0.26 ± 0.10	817 ± 337	4.28
Asp 14	0.83 ± 0.01	28 ± 4	1.75	0.56 ± 0.10	162 ± 471	13.60
Thr 22	0.93 ± 0.01	116 ± 34	6.84	0.79 ± 0.02	246 ± 148	4.02
Trp 36	0.91 ± 0.02	96 ± 28	29.32	0.57 ± 0.07	933 ± 340	2.56
Trp 36′	0.82 ± 0.02	24 ± 4	1.90	0.34 ± 0.09	1242 ± 310	15.45
Arg 38	0.85 ± 0.02	62 ± 10	0.00	0.72 ± 0.04	221 ± 175	3.40
Gly 43	0.81 ± 0.01	30 ± 3	0.49	0.54 ± 0.12	142 ± 516	5.98
Gly 46	0.87 ± 0.01	0 ± 3	2.43	0.19 ± 0.09	1207 ± 247	9.12
Ile 48	0.86 ± 0.01	11 ± 4	7.12	0.55 ± 0.02	319 ± 109	0.00
Ser 50	0.90 ± 0.02	0 ± 0	23.97	0.54 ± 0.02	234 ± 81	5.55

[a] An overall correlation time of 5.5 ns has been used for both states. The table lists the order parameter S^2, the internal correlation time τ_e, and the χ^2 goodness of fit for each residue. [b] The relaxation data obtained for the unfolded state of Ala 5 could not be fitted satisfactorily.

CONCLUSIONS

For a protein in slow exchange on the NMR time scale between folded and unfolded states, the methodology described in this paper permits the dynamics of the two states to be compared and allows the rates of the folding/unfolding transition to be determined for individual residues in the protein. Analysis of the folding transition of the drkN SH3 domain, which exists in a folded−unfolded equilibrium in aqueous buffer, reveals some variability in the values of the equilibrium constant for different residues in the molecule. While these variations appear to be significant, they correspond to small differences in thermal stability. The average rate of the folding transition of drkN SH3, 0.89 s^{-1}, is similar to previous measurements of the rates of formation of stable β-structure. The measured values of the relaxation parameters and spectral density functions of residues in the folded state indicate that the dynamical properties of the folded form of the SH3 domain are like those determined previously for other folded proteins. Thus, the folded protein behaves as a compact structure, with uniform dynamic behavior. There are differences between the relaxation parameters and spectral density functions of the unfolded and folded states indicating

that residues in the unfolded state have greater mobility and diversity of dynamic behavior. However, comparisons of the relative sizes of the values of the spectral density functions, as well as coupling constant and NOE data, suggest that the unfolded state exists as an ensemble of relatively compact structures, with motional properties like those of disordered regions in folded proteins.

ACKNOWLEDGMENT

We thank Dr. Mike Wittekind, Bristol-Myers Squibb, Princeton, NJ, for providing the coordinates of the N-terminal grb2 SH3 domain prior to publication, Dr. Ping Xu for performing calculations on the effects of chemical exchange on T_2 relaxation times measured from CPMG pulse schemes, Dr. Ranjith Muhandiram for help with the NMR spectroscopy, and Dr. Tony Pawson for providing the plasmid used to express the SH3 domain. Valuable discussions with Dr. Dennis Torchia, NIH, Bethesda, MD, are also acknowledged.

REFERENCES

Abragam, A. (1961) *Principles of Nuclear Magnetism*, Clarendon Press, Oxford.
Akke, M., Skelton, N. J., Kördel, J., Palmer, A. G., III, & Chazin, W. J. (1993) *Biochemistry 32*, 9832.
Benz, F. W., & Roberts, G. C. K. (1975) *J. Mol. Biol. 91*, 345.
Boyd, J., Hommel, U., & Campbell, I. D. (1990) *Chem. Phys. Lett. 175*, 477.
Carrington, A., & McLachlan, A. D. (1967) *Introduction to Magnetic Resonance*, Harper, New York.
Cavanagh, J., Palmer, A. G., III, Wright, P. E., & Rance, M. (1991) *J. Magn. Reson. 91*, 429.
Cheng, J.-W., Lepre, C. A., Chambers, S. P., Fulghum, J. R., Thomson, J. A., & Moore, J. M. (1993) *Biochemistry 32*, 9000.
Cheng, J.-W., Lepre, C. A., & Moore, J. M. (1994) *Biochemistry 33*, 4093.
Clore, G. M., Driscoll, P. C., Wingfield, P. T., & Gronenborn, A. M. (1990) *Biochemistry 29*, 7387.
Cross, T. A., & Opella, S. J. (1983) *J. Am. Chem. Soc. 105*, 306.
Delaglio, F. (1993) *NMRPipe System of Software*, National Institutes of Health, Bethesda, MD.
Farrow, N. A., Zhang, O., Forman-Kay, J. D., & Kay, L. E. (1994a) *J. Biomol. NMR 4*, 727.
Farrow, N. A., Muhandiram, R., Singer, A. U., Pascal, S. M., Kay, C. M., Gish, G., Shoelson, S. E., Pawson, T., Forman-Kay, J. D., & Kay, L. E. (1994b) *Biochemistry 33*, 5984.
Gruenewald, B., Nicola, C. U., Lustig, A., Schwarz, G., & Klump, H. (1979) *Biophys. Chem. 9*, 137.
Grzesiek, S., & Bax, A. (1993) *J. Am. Chem. Soc. 115*, 12593.
Gutowsky, H. S., & Saika, A. (1953) *J. Chem. Phys. 21*, 1684.
Hahn, E. L., & Maxwell, D. E. (1952) *Phys. Rev. 88*, 1070.
Hiyama, Y., Niu, C., Silverton, J. V., Bavoso, A., & Torchia, D. A. (1988) *J. Am. Chem. Soc. 110*, 2378.
Hull, W. E., & Sykes, B. D. (1975) *J. Chem. Phys. 63*, 867.
Kamath, U., & Shriver, J. W. (1989) *J. Biol. Chem. 264*, 5586.
Kay, L. E., Torchia, D. A., & Bax, A. (1989) *Biochemistry 28*, 8972.
Kay, L. E., Nicholson, L. K., Delaglio, F., Bax, A., & Torchia, D. A. (1992) *J. Magn. Reson. 97*, 359.
Kay, L. E., Xu, G.-Y., & Yamazaki, T. (1994) *J. Magn. Reson A 109*, 129.
Kördel, J., Skelton, N. J., Akke, M., Palmer, A. G., III, & Chazin, W. J. (1992) *Biochemistry 31*, 4856.
Kraulis, P. (1991) *J. Appl. Crystallogr. 24*, 946.
Kuriyan, J., & Cowburn, D. (1993) *Curr. Opin. Struct. Biol. 3*, 828.
Lipari, G., & Szabo, A. (1982a) *J. Am. Chem. Soc. 104*, 4546.
Lipari, G., & Szabo, A. (1982b) *J. Am. Chem. Soc. 104*, 4559.
Logan, T. M., Olejnickzak, E. T., Xu, R. X., & Fesik, S. W. (1993) *J. Biomol. NMR 3*, 225.
Logan, T. M., Thériault, Y., & Fesik, S. W. (1994) *J. Mol. Biol. 236*, 637.
Marion, D., Ikura, M., Tschudin, R., & Bax, A. (1989) *J. Magn. Reson. 85*, 393.
Markley, J. L., Horsley, W. J., & Klein, M. P. (1971) *J. Chem. Phys. 55*, 3604.
McConnell, H. M. (1958) *J. Chem. Phys. 28*, 430.
Neri, D., Billeter, M., Wider, G., & Wüthrich, K. (1992) *Science 257*, 1559.
Palmer, A. G., III, Cavanagh, J., Wright, P. E., & Rance, M. (1991a) *J. Magn. Reson. 93*, 151.
Palmer, A. G., III, Rance, M., & Wright, P. E. (1991b) *J. Am. Chem. Soc. 113*, 4371.
Palmer, A. G., III, Skelton, N. J., Chazin, W. J., Wright, P. E., & Rance, M., (1992) *Mol. Phys. 75*, 699.
Peng, J. W., & Wagner, G. (1992a) *J. Magn. Reson. 98*, 308.
Peng, J. W., & Wagner, G. (1992b) *Biochemistry 31*, 8571.
Shaka, A. J., Keeler, J., Frenkiel, T., & Freeman, R. (1983) *J. Magn. Reson. 52*, 335.
Shortle, D. (1993) *Curr. Opin. Struct. Biol. 3*, 66.
Sklenar, V., Torchia, D. A., & Bax, A. (1987) *J. Magn. Reson. 73*, 375.
Smallcombe, S. (1993) *J. Am. Chem. Soc. 115*, 44776.
Stone, M. J., Fairbrother, W. J., Palmer, A. G., III, Reizer, J., Saier, M. H., Jr., & Wright, P. E. (1992) *Biochemistry 31*, 4394.
Stone, M. J., Chandrasekhar, K., Holmgren, A., Wright, P. E., & Dyson, H. J. (1993) *Biochemistry 32*, 426.
Stonehouse, J., Shaw, G. L., Keeler, J., & Laue, E. D. (1994) *J. Magn. Reson. A 107*, 178.
Timasheff, S. N. (1993) *Annu. Rev. Biophys. Biomol. Struct. 22*, 67.
van Mierlo, C. P. M., Darby, N. J., Keeler, J., Neuhaus, D., & Creighton, T. E. (1993) *J. Mol. Biol. 229*, 1125.
Varley, P., Gronenborn, A. M., Christensen, H., Wingfield, P. T., Pain, R. H., & Clore, G. M. (1993) *Science 260*, 1110.
Viguera, A. R., Martínez, J. C., Filimonov, V. V., Mateo, P. L., & Serrano, L. (1994) *Biochemistry 33*, 2142.
Wittekind, M., Mapelli, C., Farmer, B. T., III, Suen, K.-L., Goldfarb, V., Tsao, J., Lavoie, T., Barbacid, M., Meyers, C. A., & Mueller, L. (1994) *Biochemistry 33*, 13531.
Zhang, O., & Forman-Kay, J. D. (1995) *Biochemistry* (in preparation).
Zhang, O., Kay, L. E., Olivier, J. P., & Forman-Kay, J. D. (1994) *J. Biomol. NMR 4*, 845.

BI942309Z